Matters Arising

Developmental Cell

Geometrical Details Matter for Mechanical Modeling of Cell Morphogenesis

Graphical Abstract

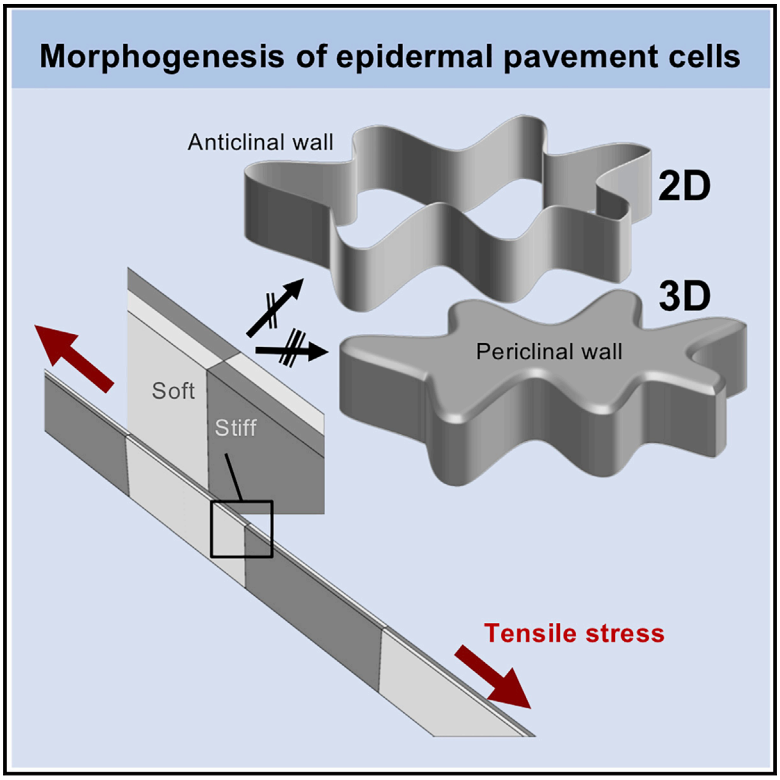

Highlights

- Model of wavy cell morphogenesis based on in-plane tension of anticlinal wall tested in 3D
- Stress predicted by the model does not match microtubule or cellulose profiles
- The periclinal walls of pavement cells are crucial in cell morphogenesis
- Simplifying assumptions in modeling approaches must be carefully validated

Authors

Amir J. Bidhendi, Anja Geitmann

Correspondence

geitmann.aes@mcgill.ca

In Brief

A mechanical model for plant pavement cell morphogenesis suggested that contiguous stiff and soft zones in the anticlinal walls can produce wavy cell borders upon tension. Bidhendi and Geitmann re-evaluate this model and challenge its function when considering 3D geometry and argue that its predictions are inconsistent with biological data.

Bidhendi & Geitmann, 2019, Developmental Cell *50*, 117–125
July 1, 2019
https://doi.org/10.1016/j.devcel.2019.05.001

CellPress

Developmental Cell
Matters Arising

Geometrical Details Matter for Mechanical Modeling of Cell Morphogenesis

Amir J. Bidhendi[1] and Anja Geitmann[1,2,*]
[1]Department of Plant Science, McGill University, Macdonald Campus, 21111 Lakeshore, Ste-Anne-de-Bellevue, QC H9X 3V9, Canada
[2]Lead Contact
*Correspondence: geitmann.aes@mcgill.ca
https://doi.org/10.1016/j.devcel.2019.05.001

SUMMARY

Morphogenesis of wavy epidermal pavement cells in plants has fascinated researchers for decades. A mechanical mechanism had been proposed in which the anticlinal cell walls, forming the in-plane cell borders, feature contiguous stiff and soft zones that generate waves upon stretching. We replicated this model as designed and also expanded on it to test its validity for three-dimensional (3D) cell geometry. Our results suggest that both the assumptions going into and the predictions arising from this hypothesis do not stand closer scrutiny and may misguide experimentalists. Unlike what the published data seem to suggest, we observed that only waves of negligible magnitude can be formed by this anticlinal stretch model and that these are virtually eliminated when full 3D geometry of the cell is considered. Further, the model produces cell wall stresses that do not match the experimental evidence.

INTRODUCTION

"Showing impossibility is the most powerful use of mathematical models: it allows hypotheses to be falsified" (Howard, 2014). In this study, we evaluate a mechanism recently proposed by Majda et al. (2017) for the formation of wavy cell borders in plant leaf epidermis, a common phenomenon in many plant species (Vőfély et al., 2019). Cells are physical objects. These microscopic units comprise structural features and are characterized by mechanical properties that are intimately related to their function. This insight has led to a rapid evolution of the field of cell mechanics and an increasingly interdisciplinary approach to biology. The mechanics lens to cell biology has resulted in the recognition that nuclear mechanics plays a role in intracellular signaling and mechanosensing (Dahl et al., 2008; Fal et al., 2017) and that cytoskeletal mechanics is a crucial element of cancer cell proliferation (Fife et al., 2014) and gene expression (Fletcher and Mullins, 2010; Mouw et al., 2014). Developmental biology, in particular, has gained significantly from combining mechanical modeling, material science, and novel imaging tools (Fayant et al., 2010; Hosseini et al., 2017).

Cell mechanics or biomechanics involve the application of mathematical, physical, and engineering concepts to biological systems. However, this approach is not without challenges. These arise from the highly complex and hierarchical organization of biological structures and are compounded by the complex mechanical properties that are typical for biomaterials. In plant development, attention to mechanics has a long tradition since the modulation of the cell wall mechanical properties and the effect of the hydraulic pressure generated by turgor are central to morphogenesis (Geitmann and Ortega, 2009; Lockhart, 1965). The emergent bio-mechanochemical properties of the cell wall are, therefore, of fundamental importance to plant cell and developmental biology (Bidhendi et al., 2019; Bidhendi and Geitmann, 2016).

Mechanical models for plants span different length scales from macromolecules to tissues and organs (Bidhendi and Geitmann, 2018). A model is a simplified representation of a system and focuses on the aspects vital to the phenomenon being investigated. Every model is inherently limited by simplifying assumptions and the quality of input parameters such as the constitutive models and boundary conditions (Bidhendi and Geitmann, 2018). These include also the geometrical aspects of the model. In the absence of feasible experimental tests allowing the determination of exact values, one must resort to educated assumptions to choose input parameters for a model. Where assumptions are made, it is sensible to test how sensitive the model outcomes are to the choice of parameters and whether certain seemingly unimportant details can safely be neglected without substantially changing the outcome. The suitability of a model can then be judged by asking whether it facilitates our understanding of complex phenomena and whether the predictions can be validated experimentally. Importantly, impactful models guide biologists toward relevant new information or novel experimental designs that benefit the quest for understanding biological functioning.

Leaf pavement cells constitute the plant epidermis and represent a particularly intriguing cell type. The tabular cells consist of two parallel periclinal walls connected by anticlinal walls lining the perimeter (border) (Figure 1A). In many plant species, the meandering borders (anticlinal walls) of these cells form interlocking protrusions (lobes) and indents (necks) that make the tissue resemble a jigsaw puzzle (Vőfély et al., 2019). Because of their complex shapes and their accessibility at the organ surface, pavement cells have become a model system for the investigation of cell development and morphogenesis in plants. The peculiar jigsaw puzzle pattern has raised developmental and

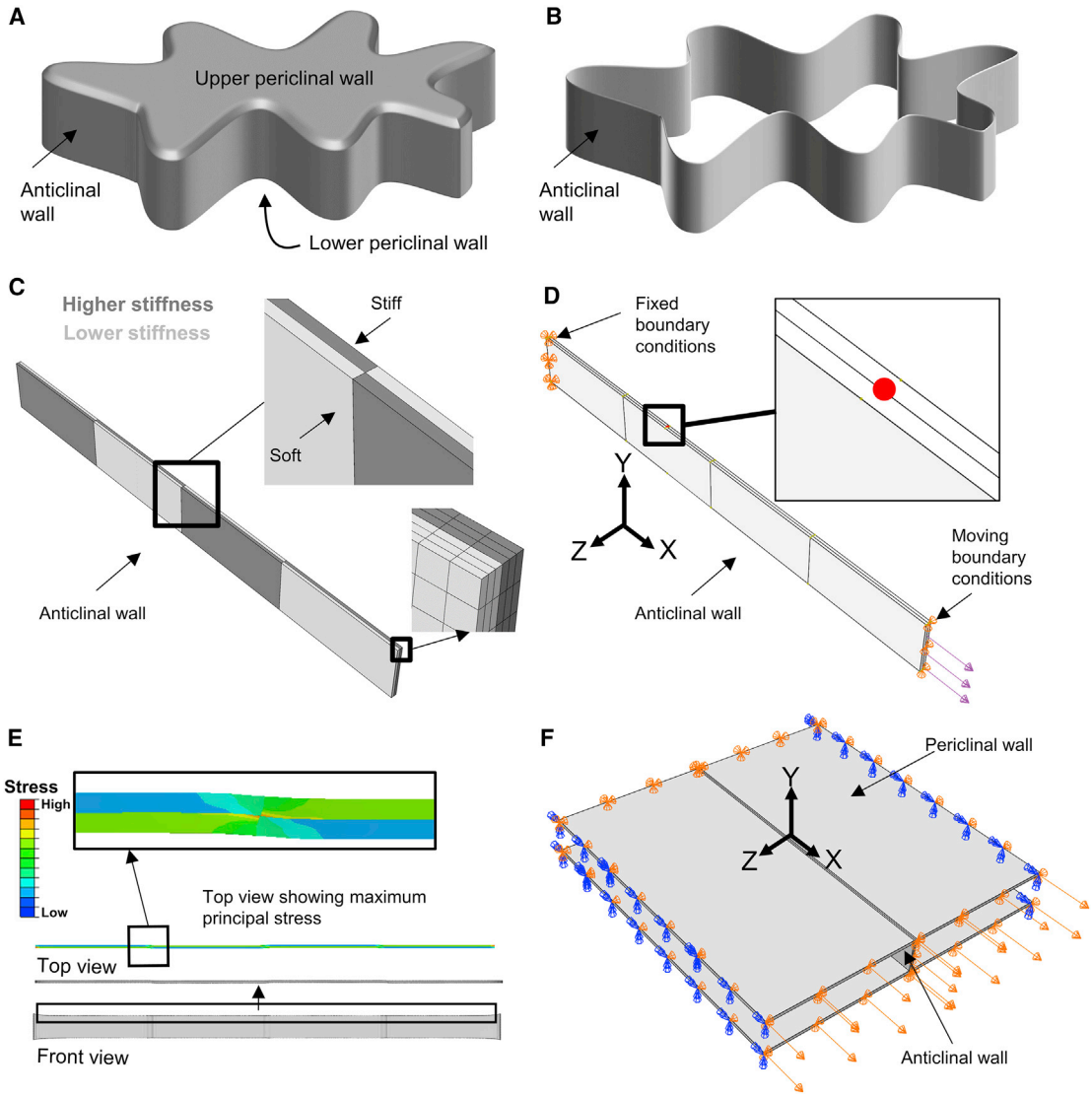

Figure 1. Finite Element Model of Geometrical Features in Plant Epidermal Pavement Cells

(A) Schematic view of a wavy pavement cell. The anticlinal walls (vertical) mark the cell borders. The two parallel periclinal walls enclose the cell at top and bottom.

(B) Description of pavement cell reduced to its lateral anticlinal walls without the periclinal walls.

(C) Anticlinal wall model consisting of a straight portion segmented into zones of elevated and decreased stiffness along and across the thickness of the wall.

(D) At one end of the anticlinal wall, fixed boundary conditions are used, and the wall is stretched at the other end. The lateral displacement (in the z direction) of the node in the middle of the length and thickness of the second wall segment (red dot) is used to measure the lobe magnitude in all models.

(E) An anticlinal wall with 1, 10, and 100 μm dimensions in thickness, height, and length, respectively, is stretched. The material behavior is hyperelastic with equivalent elastic moduli of E_{Stiff} = 100 kPa and E_{Soft} = 50 kPa, and ν = 0.3. Top view of the anticlinal wall shows the very small deformations formed in the length of the wall. Close-up of the wall deformation and maximum principal stress in the anticlinal wall shows the waves are produced because of local moments generated by the stress/strain mismatch due to material stiffness; a negligible deformation is generated, and stresses shift around the transition zones where stiffness changes.

(F) Upper and lower periclinal walls are added at the two sides of the anticlinal wall. The entire structure is fixed at one end while stretched at the other along the x direction. Symmetry boundary conditions are applied at free edges of the periclinal wall segments. Similar to the isolated anticlinal wall model, displacement of the midpoint of the second segment of the wall in z direction was measured to determine the amplitude of the waves formed in the wall.

evolutionary questions. However, *why* and *how* exactly these shapes have evolved has remained an intriguing riddle fueling intense biological and mechanical research (Armour et al., 2015; Bidhendi et al., 2019; Fu et al., 2005; Jacques et al., 2014; Majda et al., 2017; Panteris and Galatis, 2005; Sampathkumar et al., 2014; Sapala et al., 2018).

A recent paper by Majda et al. (2017) has proposed an interesting concept for the mechanics underlying the formation of the cell border undulations in pavement cells. The authors focus on the anticlinal walls (Figure 1B) and propose that these are stretched by "tissue-level forces" present in the epidermis, causing waviness because of an alternate arrangement of

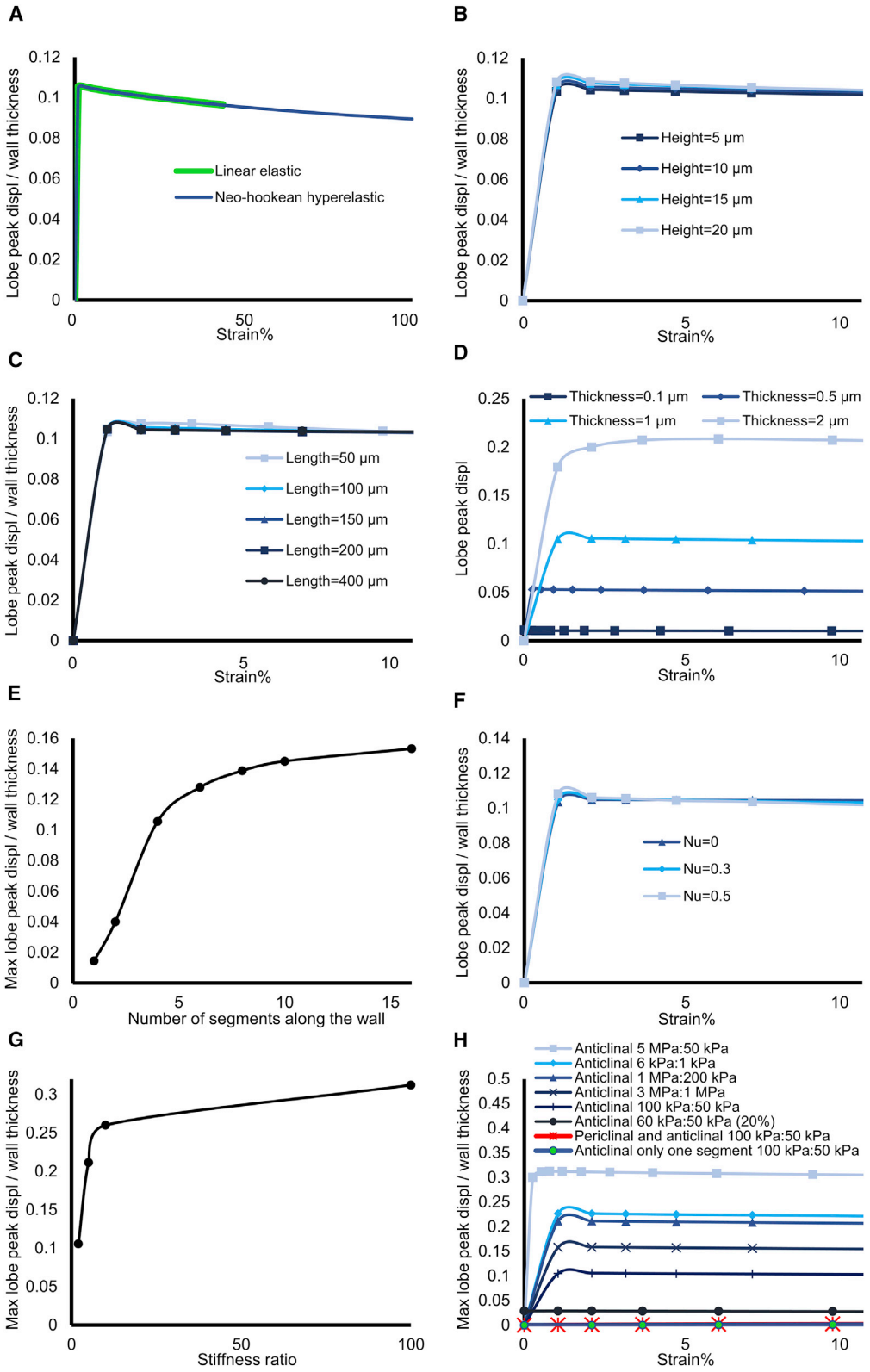

Figure 2. Simulation of Lobe Formation using a Finite Element Model Based on Alternating Stiff and Soft Regions in the Anticlinal Wall under Axial Stretch

(A) Lobe magnitude normalized by wall thickness for linear elastic (green) and neo-Hookean hyperelastic (blue) models. Comparison between models is carried out to ascertain that the results for the hyperelastic model are similar to the linear elastic model and to remain comparable with the study by Majda et al. (2017). In

(legend continued on next page)

mechanical stiffness (Figure 1C). Experimental evidence to support this mechanical concept was provided based on atomic force microscopy (AFM) indentation of resin-embedded anticlinal cell wall segments, which appeared to reflect a degree of heterogeneity in the cell wall mechanical properties. Immunohistochemical evidence was used to further corroborate material heterogeneity along the anticlinal walls. The mechanical model presented to support this notion focuses exclusively on the anticlinal walls of the pavement cells, neglecting the adjoining roof and floor periclinal walls (Figure 1B). In this study, we focus on the modeling aspects of the Majda et al. (2017) and do not discuss the other aspects such as the AFM measurements.

We were intrigued by the proposed mechanism and decided to reproduce and further analyze the model proposed by Majda et al. (2017). The finite element method is a powerful mathematical approach that is widely applied to find solutions to mechanical and structural problems with complex materials and geometries (Baker, 2012). As with all modeling approaches, simplifications and assumptions must be done sensibly. We, therefore, wanted to test whether the proposed model can generate waves, and we performed stress analysis and verified whether the simplifying assumption of neglecting the periclinal walls in a mechanical model of a pavement cell was justifiable. This question arises from the fact that Majda et al. (2017) did not make any attempt to reconcile their novel concept with previously published works that emphasize the potential importance of the periclinal wall or the spatial distribution of microtubules (used as proxy for mechanical stress) or cellulose microfibrils (Fu et al., 2005; Hamant et al., 2008; Panteris and Galatis, 2005; Sampathkumar et al., 2014).

RESULTS

Alternating Placement of Regions with Different Stiffness Produces Only Very Small Bends in the Anticlinal Wall upon Stretching

To evaluate the results published by Majda et al. (2017), we developed an isolated anticlinal wall model that, just like the one described in that paper, exhibits alternating stiff and soft regions along the wall and across the wall thickness (Figure 1C). Just as in Majda et al. (2017), the finite element mesh was sufficiently fine to represent the wall thickness by multiple volumetric elements ($N \geq 4$). As mentioned in the STAR Methods section, mesh sensitivity analysis was performed to ensure that results are independent of meshing and elements used. The base dimensions used in the model were 1, 10, and 100 μm for thickness, height, and length of the anticlinal wall, respectively. For the default model used as the base of the parametric studies, the anticlinal wall was divided into four segments along its length and in two segments in its thickness. Majda et al. (2017) reported using different stiffness ratios for soft and stiff zones with a range of Young's moduli. We used Young's moduli of 100 and 50 kPa for stiff and soft regions, respectively, and a Poisson's ratio of 0.3, as outlined in their STAR Methods. We used the mentioned dimensions and elastic constants as default values and explicitly mention if any of these values were changed. Boundary conditions were set to prevent displacement at one end of the anticlinal wall while the other end was stretched (Figure 1D). Movement perpendicular to force application was free for all sections of the wall except for the edges at the two extremities. We performed tests to rule out that the boundary conditions (displacement or rotations) at the two extremities affect the model results in any significant way. To consistently measure the amplitude of the generated waves for all models, we measured the lateral (in z direction) displacement of the middle point in length and thickness, of the second segment of the anticlinal wall (Figure 1D).

Upon stretching, the anticlinal wall made a quantitatively detectable but extremely small deformation. The very small bends are formed by the moment generated by stresses arising because of stiffness mismatch in adjacent segments (close-up in Figure 1E). Unlike the pronounced deformations illustrated in Figures 2G–2L of Majda et al. (2017), the wave amplitude in our simulations did not surpass 0.1 times the wall thickness (Figures 2A and 2H). In other words, for an anticlinal wall of 1 μm thickness, the amplitude of this curvature would be 100 nm, significantly less than its own thinnest dimension. We tested this model for axial strains up to 100% (which means stretching the wall up to double its original length). We observed that maximum wave amplitudes occur consistently at relatively small strains (~1%) (Figures 2B and 2C). To reliably test models for high deformation values, we used a hyperelastic formulation that is better suited for large deformations. We calculated the input parameters for neo-Hookean hyperelastic material behavior based on Poisson's ratio of 0.3 and the default Young's modulus values of 100 kPa and 50 kPa for stiff and soft regions,

either case, wave amplitudes in the wall remain visually indiscernible. In a 1 μm thick wall, the lobe displacement is close to 100 nm for a 100% stiffness difference between the soft and stiff regions. Maximum lobe displacements are observed to occur at small strains (~1%).

(B and C) Lobe magnitude normalized by wall thickness for different (B) heights and (C) lengths of the anticlinal wall, while other geometrical and material parameters are kept constant. Model results indicate that lobe magnitude is not sensitive to these dimensions.

(D) Lobe magnitude for different wall thickness values shows an increase in lobe magnitude at increasing thickness. However, the trend is linear, and the magnitude remains the same when the lobe displacement is normalized by the wall thickness.

(E) Increasing the number of wall segments within a given length of anticlinal wall results in increased lobe magnitude, but the trend approaches a plateau.

(F) Varying the compressibility of the elastic material by changing the Poisson's ratio does not change the lobe magnitude.

(G) Increasing the stiffness ratio between the soft and stiff regions along and across the anticlinal wall results in larger lobe displacements. However, even for ratios as high as 100 times, the lobe displacement for a wall of 1 μm thickness remains marginal.

(H) With the periclinal walls added to the anticlinal wall model or by reducing the number of stiffness segments in the isolated anticlinal wall model to one, the lobe magnitude becomes virtually zero. Similarly, the lobe displacement in the anticlinal wall model, for 20% stiffness differences reported in the experimental section of the Majda et al. (2017), is negligible. As per default, all wall models incorporate four segments along their length, except for the model with a single anticlinal wall segment. Anticlinal wall thickness is always divided into two segments with varying stiffness. Importantly, the results demonstrate that augmenting the stiffness ratio increases the lobe magnitude but that changing the absolute stiffness values does not. However, even for extreme ratios and for the free isolated anticlinal wall, the lobe magnitude remains negligible, compared to cell dimensions and even compared to wall thickness.

respectively. The hyperelastic model produced a deformation matching the wave amplitude obtained using the linear elastic model (Figure 2A). Details of the conversion between the neo-Hookean hyperelastic material and linear elastic constants are provided in the STAR Methods. From here onward, we use the hyperelastic material model, but for ease of comparison between the results, we mention the linear elastic constants that were used to calculate the input values for the hyperelastic model.

We had constructed our model using exactly the specifications provided by Majda et al. (2017), but only obtained negligible deformations that seemed to be nowhere near those presented in that paper (e.g., Figures 2D and 2G in Majda et al. (2017)). Since for some results presented in Majda et al. (2017), the input parameters or the units for the outputs were not explicitly stated, we performed a parametric study sweeping the parameter space to take into account a wide range of possible geometrical and material aspects of the model. Specifically, we varied the values for the three dimensions of the anticlinal wall, the number of wall segments within a given anticlinal wall, and the stiffness and compressibility values for the stiff and soft regions. Changing the height or length of the anticlinal wall model when keeping all the other parameters constant did not alter the wave amplitude significantly (Figures 2B and 2C). A nearly linear relationship was found between the wall thickness and wave amplitude (Figure 2D). Therefore, if the wave amplitude is normalized by the wall thickness, varying this dimension is also inconsequential in terms of the potential to generate more pronounced waves. In Majda et al. (2017), the anticlinal wall models seem to include four or six segments along the length (Figure 2G in that paper). We varied this number between 1 and 16 while keeping the other parameters at their default values. With increasing number of segments, a nonlinear increase in the lobe magnitude was observed (Figure 2E). However, the trend approached a plateau at values higher than 10, suggesting that increasing the number of contiguous regions per given length cannot generate wave magnitudes beyond a fraction of the anticlinal wall thickness. Therefore, the number of segments can also be ruled out as a putative source of difference between our results and those shown by Majda et al. (2017). Further, if the number of subregions equals one, lobe displacement becomes virtually zero (Figure 2E and 2H). Therefore, the modeling approach presented by Majda et al. (2017) does not seem to be able to explain how first-order (C-shaped) bends in the cell walls are generated, which are typical for early developmental stages in the pavement cells.

We then investigated how the Poisson's ratio of the material affects the magnitude of the waves by varying it between 0 and 0.5. As shown in Figure 2F, the effect of Poisson's ratio on wave magnitude appears negligible. Varying the stiffness ratio between the stiff and soft regions along and across the anticlinal wall, however, seemed to influence the lobe magnitudes, since different wall deformations were obtained when varying Young's moduli for stiff and soft zones between 10 kPa to 1 MPa covering a range of 1.2 to 100 times stiffness ratios. However, for all values within the tested range, even for highly exaggerated stiffness ratio values, the bends in the anticlinal walls remained negligible (Figure 2H). It should be noted that Majda et al. (2017) report rather low stiffness differentials between soft and stiff regions, as low as 20%, to be used as input of their finite element model (e.g., see Figure 2I of Majda et al. (2017)), a value that they deduce from their AFM indentation measurements (e.g., see Table 3C and bar charts in Figures 3D and 4 of Majda et al. (2017)). The outcome of a 20% stiffness difference is included in the sweep of the parameter space shown in our Figure 2H.

Interestingly, Majda et al. (2017) state, "…lowering the elastic modulus favors the bending behavior of the wall," and they show this effect in their Figure 2I. To investigate how the absolute or relative values of stiff and soft zones affect wave amplitude, we maintained a stiffness ratio of 2, varying absolute values of the elastic moduli on a range between 1 kPa to 10 GPa. Our simulations showed that for a constant stiffness ratio, no change in the lobe amplitude was generated by varying the absolute values. Our results, therefore, suggest that the absolute values are irrelevant and thus do not confirm those by Majda et al. (2017) (Figure 2I in Majda et al. (2017)). In Figure 2H, we present the maximum lobe magnitudes generated by various input parameters. In all cases, the lobe displacement or magnitude of bends generated by the anticlinal wall models remained extremely shallow and did not surpass a fraction of the cell wall thickness.

Addition of Periclinal Walls to the Stretch-Based Anticlinal Wall Model Suppresses Any Small Bends

Even small deformations might represent an initial trigger that could lead to undulation formation if enhanced by a subsequent amplification mechanism (Bidhendi et al., 2019). Therefore, we tested whether the small deformations generated in the anticlinal wall by the model proposed by Majda et al. (2017), as outlined in the previous section, would hold once the 3D structure of the plant cell is considered by adding the periclinal walls. To this end, we added the upper and lower periclinal walls to the finite element model, generating a partial segment of two adjacent cells (Figure 1F). Along the z direction, symmetry boundary conditions were applied while the walls were stretched along the x direction at one end. With all parameters kept constant, the small deformations observed earlier virtually disappeared (Figure 2H). Whether or not turgor was applied to the periclinal walls did not affect the outcome. Varying the boundary conditions, such as removing the symmetry constraint, did not significantly alter the observed lobe displacements. In our hands, the model proposed by Majda et al. (2017) is, therefore, unable to generate undulations when the periclinal walls are included.

The Stretch-Based Model Generates Unexpected Stress Patterns in the Cell Wall

We are not aware of an experimental method that allows the direct visualization of stress patterns at the cellular level. However, the orientation of microtubules is thought to be a good proxy in plant cells since these cytoskeletal elements are shown to align along known stress fields (Hamant et al., 2008; Landrein and Hamant, 2013). An additional opportunity to validate a mechanical model is, therefore, to compare the predicted stress patterns with the orientation of microtubule arrays. Evaluation of the stress pattern in the anticlinal wall

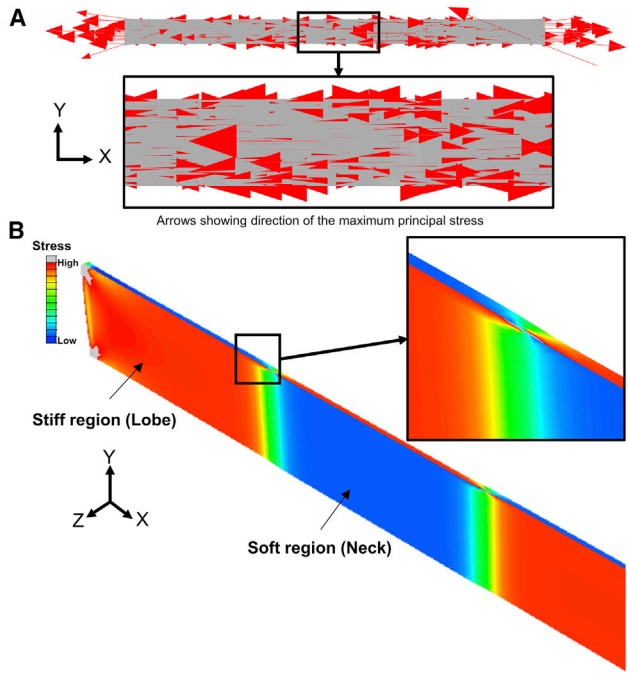

Figure 3. Stress Pattern in the Axially Stretched Anticlinal Wall

(A) Side view of the anticlinal wall showing the orientation of the maximum principal stress upon application of tensile load in x direction (red arrows).

(B) Stiffer segments form the lobe (protrusion) sides of the undulations and experience higher stresses. The resulting stresses correspond to 1% strain in a model with a stiffness ratio of 100 kPa: 50 kPa between the adjacent segments. The heatmap represents the distribution of maximum principal stress.

model was not provided by Majda et al. (2017), but our simulations allowed us to determine the same. As can be expected by the application of a tensile load in x direction, the stretch-based model predicts tensile stresses oriented along the long axis of the anticlinal wall (Figure 3A). This is inconsistent with the commonly observed orientation of microtubules underlying the anticlinal walls of pavement cells, which is transverse to the long axis of the anticlinal wall (in y direction in our coordinate system or orthogonal to the plane of the leaf) (Belteton et al., 2018; Bidhendi et al., 2019). While the actual stress pattern in the 3D structure of the cell may be more complex, the microtubule arrays seem to indicate that the predominant stress or strain pattern in the anticlinal wall is perpendicular to its long axis.

More important, however, is the side of the anticlinal wall at which higher stresses are observed. Our simulations allowed us to determine the location of elevated stresses, which in the stretched anticlinal wall model, were at the lobe side of the very small waves (Figure 3B). This, again, is inconsistent with microtubule distribution, which shows marked accumulations at the neck sides (Bidhendi et al., 2019; Fu et al., 2005; Sampathkumar et al., 2014).

DISCUSSION

Mechanical modeling of plant cells and tissues has allowed us to investigate how cells deform in response to internal and external forces and how mechanical cues correlate with physiochemical events at the subcellular level (Bidhendi and Geitmann, 2018). Inevitably, modeling requires simplifications and assumptions in the geometry, boundary conditions, and constitutive equations describing cells or tissue behavior. Examples for modeling simplifications include considering the plant cell as a thin-walled pressure vessel, assigning a linear isotropic elastic law to the material or neglecting cellularity of the tissue by treating it as a continuous material. Simplifications are performed because of various reasons such as the lack of experimental data that would be needed to inform an added complexity in the model or the removal of irrelevant features to save modeling and computation times. We acknowledge the necessity of such simplifications. However, one must ascertain that simplifications and assumptions made in the modeling process are justifiable and do not remove crucial features that have the potential to significantly affect the model results.

One of the assumptions in the model proposed by Majda et al. (2017) was the presence of "tissue-level" tensile stresses that are assumed to drive the stretching of the anticlinal walls. The concept of "tissue-level" forces in plants is introduced in several previous studies (Baskin and Jensen, 2013; Hejnowicz et al., 2000; Sampathkumar et al., 2014). In tissues such as the plant hypocotyl, where a close physical interaction between the epidermis and the densely packed internal layers exists, stresses are suggested to arise because of differences in mechanical properties and growth mismatch between the layers. Arguments for the presence of tensile forces in the epidermis are based on experiments in which the epidermis is shown to split open when cut. This behavior is attributed to forces of the inner, densely packed tissues pressing against the outermost layer (e.g., refer to Kutschera and Niklas, 2007; Savaldi-Goldstein et al., 2007). In the leaf, on the other hand, the mesophyll differentiates into a sponge-like aerenchyma, which can form large regions of limited contact between neighboring mesophyll cells and at the border between the mesophyll cells and the pavement cells of the epidermis, thus potentially reducing the influence of the former on the latter in terms of generating tissue-level stretch in the epidermis. Whether a tissue in which cells are interspersed with a significant amount of air space can exert forces in a centrifugal direction remains, therefore, to be investigated. In other words, while Majda et al. (2017) presume tensile forces in the epidermis to be a globally applicable feature, this extrapolation from other plant organs remains to be validated for the architecturally very distinct leaf. The question becomes even more acute in leaves lacking mesophyll such as *in vitro* grown mesophyll-less *Adiantum capillus-veneris* or monolayer tissues such as fern gametophytes, which nevertheless do have pavement cells with wavy borders (Armour, 2013; Korn, 1976; Panteris et al., 1994). We did not address the question of tissue forces any further in the present manuscript but chose to mention it to illustrate that it would be most helpful if modeling assumptions were justified by some detail and if they were consistent with known features and processes.

In their study, Majda et al. (2017) perfunctorily reject the possibility of cell wall buckling, a mechanical morphogen shown to be involved in shape formation of numerous cells and organs (Nerurkar et al., 2017; Taber, 1995). Instead, the

authors propose that waves are generated in the anticlinal walls of pavement cells upon stretching when alternatingly located regions of elevated stiffness are distributed along and across the walls. We first imitated the finite-element-based modeling approach focusing solely on isolated anticlinal walls as proposed by Majda et al. (2017). We showed that stretching this wall is only able to produce near imperceptible bends. The addition of periclinal walls virtually eliminates the infinitesimally small bends formed upon stretching of isolated anticlinal wall. We then performed a series of parametric studies to explore the parameter space and to ascertain that our results were not due to a particular choice of the model input parameters. We varied elastic constants of the cell wall zones, the number of the contiguous regions of stiffness variations, and the dimensions of the cell wall. Regardless of variation in input parameters, in the model developed based on the concept proposed by Majda et al. (2017), we were unable to simulate the generation of significant waves using a stretch-based wave formation mechanism. Regrettably, direct and quantitative comparison between our data for bend magnitudes and those presented by Majda et al. (2017) was impossible since the graphs provided in that paper (Figure 2I of Majda et al. (2017)) specify neither the units nor a definition of how bending of the wall was measured. From their Figure 2G, it seems as if an amplitude of at least 3 times the wall thickness was achieved in this way. Deformations in none of our simulations come remotely close to such values. If the stretching mechanism based solely on material inhomogeneities in the anticlinal wall is unable to produce the observed waviness, especially once the complete geometry of the cell is considered by addition of periclinal walls, the relevance of the proposed model for pavement cell morphogenesis must be questioned.

We considered it necessary to further assess the other outputs of the model beyond the magnitude of lobe deformation, specifically the stress state in the cell wall that accompanies the deformation. Our reproduced model afforded us the opportunity to analyze additional aspects of the predictions made by the finite element model proposed by Majda et al. (2017). The authors did not report the stresses arising upon load application, although this type of data is readily obtained using the finite element method. Our reconstruction of their model shows that in the very small bends that are created in the isolated anticlinal wall model, stresses on the lobe side of the anticlinal wall are more elevated than on the neck side. This observation is of importance since it is challenging to reconcile it with the available literature. Sampathkumar et al. (2014) and Bidhendi et al. (2019) showed that periclinal walls of pavement cells, when inflated by turgor, experience elevated stresses at the location of necks. This is consistent with the observed cytoskeletal polarization in these cells (Armour et al., 2015; Bidhendi et al., 2019; Fu et al., 2005; Zhang et al., 2011). The arrangement of plant microtubules is known to be strongly driven by mechanical stress or strain fields experienced at the cell wall level (Landrein and Hamant, 2013; Uyttewaal et al., 2012). The experimentally observed accumulation of microtubules at necks is consistent with the finite-element-based prediction of stress pattern predicted by Sampathkumar et al. (2014) and Bidhendi et al. (2019) but not with the stress pattern predicted by the anticlinal wall model based on the concept proposed by Majda et al. (2017). No attempt was made by Majda et al. (2017) to reconcile their proposed model with the contrasting and strikingly different outcomes in terms of wall stress in Sampathkumar et al. (2014) or with the morphogenetic concept proposed by Panteris and Galatis (2005). The consequences of this inconsistency are even farther reaching. An accumulation of microtubules is generally translated into an increased deposition of cellulose microfibrils and hence a local stiffening of the wall. This was shown to be the case by Sampathkumar et al. (2014), where the predicted stress pattern in the periclinal neck regions was shown to correlate with local patterns of wall stiffening measured by indentation. The cortical microtubules observed in the neck regions of periclinal walls are thought to extend into the depth of the anticlinal wall (Panteris and Galatis, 2005; Zhang et al., 2011). As we show in Bidhendi et al., 2019, this does indeed translate into an accumulation of cellulose microfibrils in the anticlinal wall, as is consistent with predictions made by (Panteris et al., 1994 and Panteris and Galatis, 2005). It, therefore, remains to be investigated how this expected cellulose-based stiffening at the neck side can be reconciled with the softer material in the same region that Majda et al. (2017) propose to have observed experimentally. Several considerations can be made, ranging from the reliability of stiffness measurements of resin-embedded material to a lack of sufficiently time-resolved data to correlate a specific side of a bend to observed wall stiffness heterogeneity. Further studies are certainly warranted to investigate the experimental aspect of Majda et al. (2017), but these are beyond the scope of this paper.

Another limitation of the model by Majda et al. (2017) is the fact that the stretch-induced wave formation based on alternating stiffness distribution is unable to produce pronounced first-order bends (a simple curvature such as a C-shaped arc). This is the case even if the isolated anticlinal wall model is considered in the absence of periclinal walls (Figure 2H). It is important to note that first-order bends are a common occurrence in early stages of pavement shape formation and would, therefore, remain inexplicable by the concept model proposed by Majda et al. (2017). In summary, clearly, more research is warranted to establish consistent mechanical models that explain the morphogenesis of pavement cells.

The pavement cell case illustrates pitfalls of modeling when focusing solely on a selected aspect of the cell geometry. The overall shape and construction of the cell may be too relevant to be neglected, and misleading predictions are bound to arise through a reductionist approach without proper investigation of the simplifying assumptions. Modeling relies on simplifications and typically accounts only for features that matter for the outcome. The simplifications and assumptions need to be evaluated prior to drawing conclusions, as "mathematical modeling can be less useful or even misleading if used inappropriately, for example, when a microscope is used to study stars." (Ganusov, 2016). Predictions made by models that generate attractive simulation outcomes only under conditions that are far removed from the reality or oversimplified risk guiding biologists toward an erroneous path resulting in a snowball effect that can become hard to contain.

STAR★METHODS

Detailed methods are provided in the online version of this paper and include the following:

- KEY RESOURCES TABLE
- LEAD CONTACT AND MATERIALS AVAILABILITY
- METHOD DETAILS
  - Finite Element Modeling Procedures
- DATA AND CODE AVAILABILITY

ACKNOWLEDGMENTS

This project was supported by a Discovery grant from the Natural Sciences and Engineering Research Council of Canada (NSERC) and by the Canada Research Chair Program.

AUTHOR CONTRIBUTIONS

A.J.B. and A.G. designed the study. A.J.B. developed the models. A.J.B. and A.G. analyzed the results and wrote the manuscript.

DECLARATION OF INTERESTS

The authors declare no competing interests.

Received: November 30, 2018
Revised: March 18, 2019
Accepted: April 30, 2019
Published: July 1, 2019

REFERENCES

Abaqus Theory Manual. (2018). Dassault Systèmes (Simulia Corporation).

Armour, W.J. (2013). Development of pavement cell shape in *Arabidopsis* cotyledons, PhD thesis (University of Sydney).

Armour, W.J., Barton, D.A., Law, A.M., and Overall, R.L. (2015). Differential growth in periclinal and anticlinal walls during lobe formation in *Arabidopsis* cotyledon pavement cells. Plant Cell *27*, 2484–2500.

Baker, A.J. (2012). Finite Elements: Computational Engineering Sciences (John Wiley & Sons).

Baskin, T.I., and Jensen, O.E. (2013). On the role of stress anisotropy in the growth of stems. J. Exp. Bot. *64*, 4697–4707.

Belteton, S.A., Sawchuk, M.G., Donohoe, B.S., Scarpella, E., and Szymanski, D.B. (2018). Reassessing the roles of PIN proteins and anticlinal microtubules during pavement cell morphogenesis. Plant Physiol. *176*, 432–449.

Bidhendi, A.J., Altartouri, B., Gosselin, F., and Geitmann, A. (2019). Mechanical stress initiates and sustains the morphogenesis of wavy leaf epidermal cells. BioRxiv. https://doi.org/10.1101/563403.

Bidhendi, A.J., and Geitmann, A. (2016). Relating the mechanics of the primary plant cell wall to morphogenesis. J. Exp. Bot. *67*, 449–461.

Bidhendi, A.J., and Geitmann, A. (2018). Finite element modeling of shape changes in plant cells. Plant Physiol. *176*, 41–56.

Dahl, K.N., Ribeiro, A.J., and Lammerding, J. (2008). Nuclear shape, mechanics, and mechanotransduction. Circ. Res. *102*, 1307–1318.

Fal, K., Asnacios, A., Chabouté, M.E., and Hamant, O. (2017). Nuclear envelope: a new frontier in plant mechanosensing? Biophys. Rev. *9*, 389–403.

Fayant, P., Girlanda, O., Chebli, Y., Aubin, C.E., Villemure, I., and Geitmann, A. (2010). Finite element model of polar growth in pollen tubes. Plant Cell *22*, 2579–2593.

Fife, C.M., McCarroll, J.A., and Kavallaris, M. (2014). Movers and shakers: cell cytoskeleton in cancer metastasis. Br. J. Pharmacol. *171*, 5507–5523.

Fletcher, D.A., and Mullins, R.D. (2010). Cell mechanics and the cytoskeleton. Nature *463*, 485–492.

Fu, Y., Gu, Y., Zheng, Z., Wasteneys, G., and Yang, Z. (2005). *Arabidopsis* interdigitating cell growth requires two antagonistic pathways with opposing action on cell morphogenesis. Cell *120*, 687–700.

Ganusov, V.V. (2016). Strong inference in mathematical modeling: a method for robust science in the twenty-first century. Front. Microbiol. *7*, 1131.

Geitmann, A., and Ortega, J.K. (2009). Mechanics and modeling of plant cell growth. Trends Plant Sci. *14*, 467–478.

Hamant, O., Heisler, M.G., Jönsson, H., Krupinski, P., Uyttewaal, M., Bokov, P., Corson, F., Sahlin, P., Boudaoud, A., Meyerowitz, E.M., et al. (2008). Developmental patterning by mechanical signals in *Arabidopsis*. Science *322*, 1650–1655.

Hejnowicz, Z., Rusin, A., and Rusin, T. (2000). Tensile tissue stress affects the orientation of cortical microtubules in the epidermis of sunflower hypocotyl. J. Plant Growth Regul. *19*, 31–44.

Hosseini, H.S., Garcia, K.E., and Taber, L.A. (2017). A new hypothesis for foregut and heart tube formation based on differential growth and actomyosin contraction. Development *144*, 2381–2391.

Howard, J. (2014). Quantitative cell biology: the essential role of theory. Mol. Biol. Cell *25*, 3438–3440.

Jacques, E., Verbelen, J.-P., and Vissenberg, K. (2014). Review on shape formation in epidermal pavement cells of the *Arabidopsis* leaf. Funct. Plant Biol. *41*, 914–921.

Korn, R.W. (1976). Concerning the sinuous shape of leaf epidermal cells. New Phytol. *77*, 153–161.

Kutschera, U., and Niklas, K.J. (2007). The epidermal-growth-control theory of stem elongation: an old and a new perspective. J. Plant Physiol. *164*, 1395–1409.

Landrein, B., and Hamant, O. (2013). How mechanical stress controls microtubule behavior and morphogenesis in plants: history, experiments and revisited theories. Plant J. *75*, 324–338.

Lockhart, J.A. (1965). An analysis of irreversible plant cell elongation. J. Theor. Biol. *8*, 264–275.

Majda, M., Grones, P., Sintorn, I.M., Vain, T., Milani, P., Krupinski, P., Zagórska-Marek, B., Viotti, C., Jönsson, H., Mellerowicz, E.J., et al. (2017). Mechanochemical polarization of contiguous cell walls shapes plant pavement cells. Dev. Cell *43*, 290–304.e4.

Mouw, J.K., Yui, Y., Damiano, L., Bainer, R.O., Lakins, J.N., Acerbi, I., Ou, G., Wijekoon, A.C., Levental, K.R., Gilbert, P.M., et al. (2014). Tissue mechanics modulate microRNA-dependent PTEN expression to regulate malignant progression. Nat. Med. *20*, 360–367.

Nerurkar, N.L., Mahadevan, L., and Tabin, C.J. (2017). BMP signaling controls buckling forces to modulate looping morphogenesis of the gut. Proc. Natl. Acad. Sci. U S A *114*, 2277–2282.

Panteris, E., Apostolakos, P., and Galatis, B. (1994). Sinuous ordinary epidermal cells: behind several patterns of waviness, a common morphogenetic mechanism. New Phytol. *127*, 771–780.

Panteris, E., and Galatis, B. (2005). The morphogenesis of lobed plant cells in the mesophyll and epidermis: organization and distinct roles of cortical microtubules and actin filaments. New Phytol. *167*, 721–732.

Sampathkumar, A., Krupinski, P., Wightman, R., Milani, P., Berquand, A., Boudaoud, A., Hamant, O., Jönsson, H., and Meyerowitz, E.M. (2014). Subcellular and supracellular mechanical stress prescribes cytoskeleton behavior in *Arabidopsis* cotyledon pavement cells. Elife *3*, e01967.

Sapala, A., Runions, A., Routier-Kierzkowska, A.L., Das Gupta, M.D., Hong, L., Hofhuis, H., Verger, S., Mosca, G., Li, C.B., Hay, A., et al. (2018). Why plants make puzzle cells, and how their shape emerges. Elife *7*, e32794.

Savaldi-Goldstein, S., Peto, C., and Chory, J. (2007). The epidermis both drives and restricts plant shoot growth. Nature *446*, 199–202.

Taber, L.A. (1995). Biomechanics of growth, remodeling, and morphogenesis. Appl. Mech. Rev. *48*, 487–545.

Uyttewaal, M., Burian, A., Alim, K., Landrein, B., Borowska-Wykręt, D., Dedieu, A., Peaucelle, A., Ludynia, M., Traas, J., Boudaoud, A., et al. (2012). Mechanical stress acts via katanin to amplify differences in growth rate between adjacent cells in *Arabidopsis*. Cell *149*, 439–451.

Vőfély, R.V., Gallagher, J., Pisano, G.D., Bartlett, M., and Braybrook, S.A. (2019). Of puzzles and pavements: a quantitative exploration of leaf epidermal cell shape. New Phytol. *221*, 540–552.

Zhang, C., Halsey, L.E., and Szymanski, D.B. (2011). The development and geometry of shape change in *Arabidopsis thaliana* cotyledon pavement cells. BMC Plant Biol. *11*, 27.

STAR★METHODS

KEY RESOURCES TABLE

RESOURCE	SOURCE	IDENTIFIER
Software and Algorithms		
Abaqus 2018	Dassault Systèmes, Simulia	https://www.3ds.com/products-services/simulia/products/abaqus/

LEAD CONTACT AND MATERIALS AVAILABILITY

Further information and requests for resources should be directed to, and will be fulfilled by, the Lead Contact, Anja Geitmann (geitmann.aes@mcgill.ca).

METHOD DETAILS

Finite Element Modeling Procedures

To investigate the paradigm suggested by Majda et al. (2017), 3D models of the isolated anticlinal wall and combined anticlinal and periclinal walls were developed. Default dimensions for the anticlinal wall were 1, 10 and 100 μm in thickness, height, and length, respectively. We verified that the dimensions of the anticlinal or periclinal wall models do not affect the outcome. Nevertheless, throughout the study we specifically adopted geometrical and material inputs that would allow for our simulations to remain comparable with those by Majda et al. (2017). By default, the anticlinal wall models were divided into four contiguous regions (see Figure 2G of Majda et al. (2017)), along their length and into half in their thickness (Figure 1C). This allowed us to assign alternating material properties along and across the anticlinal wall as done by Majda et al. (2017). We first used linear elastic material behavior to study the model. For large deformations, we then used a hyperelastic model for the rest of the study. We ascertained that the Neo-Hookean hyperelastic model produces the same deformations as the linear elastic model with input parameters calculated from their linear elastic equivalents. Hyperelastic models are defined by strain energy potential functions. Neo-Hookean hyperelastic material model is a simple hyperelastic model with the strain energy potential, $U(\varepsilon)$, defined as (Abaqus Theory Manual, 2018):

$$U = C_{10}(\bar{I}_1 - 3) + \frac{1}{D_1}(J^{el} - 1)^2$$

Where U is the strain energy per unit of reference volume. C_{10} and D_1 are material parameters. $\bar{I}_1$ is the first deviatoric strain invariant:

$$\bar{I}_1 = \bar{\lambda}_1^{\,2} + \bar{\lambda}_2^{\,2} + \bar{\lambda}_3^{\,2}.$$

$\bar{\lambda}_i$ are the deviatoric stretches, $\bar{\lambda}_i = J^{-\frac{1}{3}}\lambda_i$. λ_i are the principal stretches. J is the total volume ratio. J^{el} is elastic volume ratio. For cases that the hyperelastic model was used, to calculate the model parameters from the linear elastic parameters, the constants C_{10} and D_1 for the Neo-Hookean hyperelastic model can be calculated as:

$$C_{10} = \frac{\mu_0}{2} \text{ and } D_1 = \frac{2}{K_0};$$

where μ_0 and K_0 correspond to initial shear and bulk moduli, respectively. In many studies, the elastic parameters are given in terms of Young's modulus E and Poisson's ratio ν. If these values are provided, the initial shear modulus, μ_0 and the bulk modulus are:

$$\mu_0 = \frac{E}{2(1+\nu)} \text{ and } K_0 = \frac{E}{3(1-2\nu)}$$

It can be seen that for values of Poisson's ration approaching 0.5, the bulk modulus takes large numbers.

For the model boundary conditions, one end of the anticlinal wall structure was fixed, and the other end was stretched. To present a more realistic cell geometry, upper and lower periclinal walls were added on two sides of an anticlinal wall, representing two half cells. In this case, the symmetry boundary conditions were applied to the free edges of the periclinal walls. The displacement boundary conditions were also extended to encompass the periclinal walls cross-sections. As to whether the deformation was produced in a force or displacement control approach, we did not observe a significant change in the outcome when either the force or displacement boundary conditions were applied at the end of the wall that is pulled.

Abaqus 2018 finite element package was used for the creation of the geometries, meshing and post-processing. Geometries were discretized using second order, reduced integration hybrid C3D20RH solid finite elements and mesh sensitivity analysis was performed for each model. Mesh sensitivity analysis was carried out to ensure that the results do not depend on the type and number of elements used in the model.

DATA AND CODE AVAILABILITY

Requests for data should be directed to, and will be fulfilled by, the Lead Contact, Anja Geitmann (geitmann.aes@mcgill.ca).